

# 1 Balloon drift estimation and improved position estimates for 2 radiosondes

3 Ulrich Voggenberger<sup>1</sup>, Leopold Haimberger<sup>1</sup>, Federico Ambrogio<sup>1</sup>, Paul Poli<sup>2</sup>

4 <sup>1</sup>Department of Meteorology and Geophysics, University of Vienna, Vienna, 1090, Austria

5 <sup>2</sup>European Centre for Medium-Range Weather Forecasts, Bonn, Germany

6 *Correspondence to:* Ulrich Voggenberger (ulrich.voggenberger@univie.ac.at)

## 7 **Abstract.**

8 When comparing model output with historical radiosonde observations, it is usually assumed that the radiosonde has risen  
9 exactly above its starting point and has not been displaced by the wind. This has changed only relatively recently with the  
10 availability of Global Navigation Satellite System (GNSS) receivers aboard the radiosondes in the late-1990s, but even then  
11 the balloon trajectory data were often not transmitted, although this information was the basis for estimating the wind in the  
12 first place. Depending on the conditions and time of year, radiosondes can sometimes drift a few hundred kilometres,  
13 particularly in the mid-latitudes during the winter months. The position errors can lead to non-negligible representation  
14 errors when the corresponding observations are assimilated.

15 This paper presents a methodology to compute changes in the balloon position during its vertical ascent, using only limited  
16 information, such as the vertical profile of wind contained in the historical observation reports. The sensitivity of the method  
17 to various parameters is investigated, such as the vertical resolution of the input data, the assumption about vertical ascent  
18 speed of the balloon, and the departure of the surface of the Earth from a sphere. The paper considers modern GNSS sonde  
19 data reports for validation, for which the full trajectory of the balloon is available, alongside the reported wind. Evaluation is  
20 also conducted by comparison with ERA5 and by conducting low-resolution data assimilation experiments. Overall, the  
21 results indicate that the trajectory of the radiosonde can be accurately reconstructed from original data of varying vertical  
22 resolution and that the more accurate balloon position reduces representation errors, and, in some cases, also systematic  
23 errors.

## 24 **1 Introduction**

25

26 Prior to the availability of remote sensing techniques, upper-air measurements of air motions were widely collected using  
27 Lagrangian perspectives, with weather balloons (e.g., Dutton, 1986). The uncertainty of such upper-air observations depends  
28 not only on the measurements themselves but also on the availability and quality of associated metadata and measurement  
29 position: this is generally associated with so-called representation errors (e.g., Kitchen, 1989). As weather balloons drift with  
30 the wind during their travel, including ascent, they can thus be displaced over large distances (**Figure 1**), in some cases  
31 more than 400 km from their launch base (e.g., Seidel et al., 2011). Precise knowledge of the balloon position is particularly  
32 important in regions of sharp horizontal gradients, e.g. near mountain ranges or near jet streams. Tschannett (2003) and  
33 Steinacker et al. (2005) noted that apparent superadiabatic vertical lapse rates in Föhn events disappeared after the balloon  
34 displacement had been taken into account. For operational monitoring, detailed information regarding the balloon trajectory  
35 was generally not recorded or not transferred via the data distribution networks until the advent of Global Navigation  
36 Satellite Systems (GNSS). Even later, when GNSS sensors became available, the information collected was often not  
37 transmitted, although the wind data was calculated directly from it (WMO, 2021), as there was no available space in the  
38 alphanumeric codes. This became possible with the (ongoing) migration from alphanumeric codes to Binary Universal Form  
39 for the Representation of meteorological data (BUFR), allowing also the reporting of many more levels in the vertical  
40 (Ingleby et al., 2016). Only since the 2000s efforts have been made to take into account the balloon drift in modern  
41 observation processing of GNSS sondes, with beneficial results (e.g., Keyser, 2000; Laroche and Sarrazin, 2013; Ingleby et  
42 al., 2018).

43

44 Radiosonde measurements are used in a variety of applications, including near-real-time by forecasters and Numerical  
45 Weather Prediction (NWP), but also for air pollution or other scientific investigations, including climate monitoring (e.g.,  
46 Dabberdt and Turtiainen, 2015). The production of climate reanalyses that directly assimilate radiosonde observations, such  
47 as ERA5 (Hersbach et al. 2020), is expected to benefit from more accurate historical balloon position data, similarly to  
48 NWP. In this regard, the location precision of the assimilated measurements should be commensurate with the horizontal  
49 resolution of next-generation reanalyses (~10 to 20 km globally, e.g., Hersbach et al., 2022). At such resolutions, assuming  
50 vertical ascents for a balloon that is displaced by a couple of hundred kms would amount to comparing the balloon  
51 measurements with model values that are 10 or more grid boxes away, which is clearly suboptimal. Resolving this situation  
52 requires, for historical soundings, to reconstruct the balloon trajectories from the little information that is available (Stohl,  
53 1998). In many cases, this information only consists in the vertical profile of wind, as discussed later in the paper.

55 Section 2 describes the data and a method to calculate the balloon drift from historical radiosonde ascent data. Details of the  
56 technical implementation, with python code and test data, are provided in section 3. Section 4 presents validation results,  
57 including several sensitivity analyses to explore the robustness and accuracy of the approach. Sections 5 and 6 show

5

6

58 evaluation results, using two different approaches, whereby the beneficial impact of the more accurate balloon position is  
59 demonstrated. Section 7 includes a discussion and conclusions.

## 60 **2 Data and methodology**

61

### 62 **2.1 Radiosonde data**

63 Radiosonde data used in this work are obtained from the Integrated Global Radiosonde Archive (IGRA), Version 2 (Durre et  
64 al., 2016) and via the Copernicus Climate Change Service (C3S) Climate Data Store (CDS). High-resolution radiosonde data  
65 used for validation are obtained in BUFR format from the National Centers for Environmental Information Radiosonde  
66 Archive (NOAA NCEI).

67

68 The quality of the available wind data depends on their encoding and the method used to track the balloons. Measuring  
69 techniques for upper-air winds have changed significantly over time, with a clear general trend towards improvements in  
70 quality, thanks to removal of procedural errors, in particular (e.g., Crutcher, 1979), noting also improvements in the accuracy  
71 of encoding, with evolution of the data formats. All these changes are described in the WMO Publication Nr. 8, Guide to  
72 Meteorological Instruments and Methods of Observation, published since 1954 by the WMO Commission for Instruments  
73 and Methods of Observation (CIMO; WMO, 2021). Regarding changes in the measurements of wind and balloon positions,  
74 there are three important distinctions to be made.

75

76 The first distinction concerns the sensing apparatus: non-GNSS versus GNSS sondes. Early observations used only ground-  
77 based tracking, e.g., by theodolite, which was fairly accurate but could lose the balloon early during cloudy or high wind  
78 speed conditions, and relied on an assumed ascent rate if, like in most cases, a single theodolite was used (e.g., Favà et al.,  
79 2021). From the mid-1950s onward, radar tracking or radio-positioning of the radiosonde became standard. Wind  
80 components were then calculated from the measured position and time differences.

81 In the 1990s, GNSS modules were introduced to track the horizontal and vertical position of the sensor at high frequency,  
82 thanks to improvements and miniaturisation of the electronics. The resulting data were then used to calculate the wind  
83 variables, but the position data were not transmitted to the global network and are therefore not available in global databases  
84 in most cases until 2014.

85 The higher frequency of observations exchanged in recent years can expose the pendulum motion of the sonde beneath the  
86 balloon in its observed position (Ingleby et al, 2022). In our experimental cases, we did not observe any significant effect of  
87 the pendulum motion, its magnitude being generally much smaller than the wind advection displacements, suggesting it does  
88 not appear to need to be taken into account to first order.

10

89

90 The second aspect is the determination of altitude. Prior to GNSS observations, altitude was determined by three different  
91 methods: ascent speed estimation, pressure sensors, and vertical radar or radio-positioning, with continued efforts to increase  
92 the quality of observations over time. Ascent speed can be affected by many factors, and Murillo et al. (2005) estimated a  
93 scatter in linear ascent rates of about 5% about the mean value for pilot balloons, after using double theodolites to conduct  
94 measurements to measure the balloon height during ascent.

95

96 The third aspect is the data format used for transmission. Essentially two main message systems have been used to transmit  
97 the observed radiosonde data: Traditional Alphanumeric Code (TAC) and BUFR. The main difference is that BUFR allows  
98 not only for a much higher vertical resolution (up to 1 second frequency, corresponding to approximately 5 m altitude  
99 difference) but also for a higher coding precision. The BUFR messages report wind direction with a resolution of 1-degree,  
100 whereas TAC messages report wind direction to the nearest 5-degrees. In addition, time and three-dimensional position  
101 information is only transmitted via BUFR but not via TAC. TAC messages typically also include data only on mandatory  
102 and significant levels. Mandatory levels are a set of predefined pressure levels. Significant levels for wind are added as  
103 needed before transmission so that the wind speed does not deviate by more than 5 m/s from linearly-interpolated values,  
104 according to the above-cited WMO CIMO guide.

105 There are also thermodynamically significant levels, which refer to specific levels of atmospheric pressure at which  
106 significant changes in temperature, humidity or other thermodynamic properties occur. Most transmitted radiosonde profiles  
107 include some of these.

## 108 **2.2 Quality control**

109 The following steps are taken to exclude outliers:

- 110 • For wind speed, we applied a range check, with wind speed limited to 150 m/s, a value that is rarely reached, even  
111 in strong upper-level jets.
- 112 • For temperature, needed for geopotential calculations, we relied on the IGRA2 quality control (Durre et al. 2018)  
113 that already removes gross errors. A range check was also applied, with temperature limited to between 173 and  
114 373 K, to verify that the data were read correctly and avoid possible encoding errors in the messages.

115 Observations that fall outside these limits are not processed further, to avoid degrading the quality of the output (balloon  
116 trajectory).

117 It was investigated whether additional quality control measures would improve performance and the validation of the RMSE  
118 differences discussed in section 5. To improve outlier removal, we filtered the observations based on the 1st and 99th  
119 percentiles of the differences observations minus ERA5 forecast (these differences are called background departures  
120 afterwards). This was completed in two stages: once for each level, and then again for the entire set of available wind speed  
121 and temperature data. However, neither of the two versions improved the RMSE differences. Rather, we found that the

11

12

122 background departures were often large enough to be discarded just in the interesting cases of strong but plausible  
123 displacements. The reason was not always the displacements themselves but also the fact that large lateral displacements can  
124 lead to large height errors in profiles from non-GNSS Russian radiosondes, since those have no pressure sensor but rely on  
125 radar heights (Kats et al. , 2005). However even for these sondes, we found that taking into account the balloon drift reduces  
126 the differences to the ERA5 background forecasts.

127 The results presented in section 6 include the standard quality controls applied during data assimilation experiments, as  
128 detailed in the technical documentation published by ECMWF (2023).

129

130 Filtering radiosonde data before the displacement calculation based on the number of available observations per profile is  
131 recommended. A profile should not be too coarse and should not start too high above the ground. For the experiments  
132 conducted in this study, the limit for the initial observation was set at 1500 m above the release station height.

### 133 **2.3 Estimation of the balloon trajectory**

134 The balloon position is calculated relative to the launch position (so-called base coordinates), as latitude displacement and  
135 longitude displacement (decimal degrees). For each vertical level, these two values can be added to the base coordinates to  
136 obtain the new (latitude, longitude) position at the given level. The same approach applies to the reconstruction of the  
137 measurement times at all levels. This practice conforms to the BUFR encoding standard.

138

139 For the position calculation, the same simple physical laws that have been used to derive the reported wind components are  
140 applied. Only a few initial parameters are necessary for this:

141

- 142 • station coordinates or starting point of the sonde, (latitude and longitude) ;
- 143 • wind vector (zonal and meridional components, noted respectively  $u$  and  $v$ ), measured by the sonde at different  
144 pressure levels;
- 145 • measurement time ( $t$ ) at different pressure levels.

146

147 These variables enable calculation of how long the sonde was exposed to horizontal wind, and therefore can be used to  
148 estimate the displacement of the sonde.

149 Especially older datasets often only contain the starting time of the ascent, time information is not available for any of the  
150 reported pressure levels.

151 To estimate the time elapsed since the release of the balloon, three variables are needed:

152

- 153 • the reported pressure levels (generally available from radiosondes) or heights (generally available from so-called  
154 PILOT balloons, also called PIBAL),

- 155 ● the sonde ascent speed.
- 156 ● the surface pressure or station height (not strictly needed for displacement calculation since first level is typically
- 157 reported quite close to the surface)

158

159 PILOT or PIBAL profiles provide an estimate of height at each level, from which the time at each level can be reconstructed,  
160 assuming a given ascent speed. However, for multivariate soundings (radiosondes reporting temperature and wind), observed  
161 pressure is often the only information available regarding the radiosonde vertical position. In such a case, the pressure profile  
162 needs to be transformed to a height profile. This can be done assuming a piecewise constant temperature gradient between  
163 the levels in the profile. The calculation of the vertical gradient of temperature with respect to altitude from the vertical  
164 gradient of temperature with respect to pressure is shown below in **Formulae 1** and **2**. Subsequently, **Formula 3** indicates  
165 how this information is used to determine the heights of all pressure levels. If the height information is already available (e.g.  
166 PILOT data), those steps can be skipped.

167

168 The vertical resolution of the available data varies. While early ascents often contain even less than the mandatory levels (16  
169 levels), recent data in high resolution BUFR are available on 3000 levels or more. The sensitivity of displacement  
170 calculations to vertical resolution is investigated later in this paper.  
171 If a single mandatory level is missing within the ascent range, then the displacements are not calculated; we consider that too  
172 much information is missing in such a case. If a level was not mandatory in historical data (e.g. 70 hPa, 250 hPa, 925 hPa),  
173 this rule does not apply to the data. However, an early termination of the vertical ascent is not an issue, then the  
174 displacements are only calculated up to the highest available level.

175

176 The determination of the sonde's ascent speed is more uncertain. It depends on some variables that are poorly determined or  
177 unknown, such as the air vertical wind speed and the weight to buoyancy ratio of the probe and the balloon. Deviations in the  
178 filling level of the balloon, the air resistance of the balloon skin, as well as the ambient temperature and the balloon gas  
179 temperature further influence the ascent speed. A review of some of these factors was made by Favà et al. (2021).

180

181 Using data from recent sondes, our study of the data with known altitude time series indicates that the rate of ascent varies  
182 mostly between 2 and 10 m/s. Within this large range, **Figure 2** shows that the mode of the distribution of ascent speeds is  
183 around 5 m/s. **Table 1** further indicates that the interquartile range is 2 m/s (i.e., from 4 m/s to 6 m/s). These findings are  
184 consistent with other sources (e.g., Seidel et al., 2011). These statistics represent global fluctuations in the ascent speed of  
185 weather balloons.

186

187 Over short time scales, **Figure 3** indicates the vertical velocity of the probe fluctuates substantially. This is true both within a  
188 single ascent and also between different ascents. Near the ground and above the tropopause the fluctuations are largest.

189

190 Given the considerations above for historical balloons, one must recognize that the vertical speed can only be estimated in  
191 most cases, and will always lead to significant deviations as compared to measurements obtained from high-resolution data.  
192 Note the high vertical resolution shown in **Figure 3** is hardly reached in ascents before the year 2000. This also means that if  
193 only mandatory levels are available, the fluctuations in average ascent speed at each available level are smaller, due to the  
194 longer averaging intervals.

195

196 **Figure 2** and **Figure 3** show that an assumed ascent rate of 5 m/s agrees well with the observed mean value. To counteract  
197 the effects of this fluctuating parameter, an attempt was made to use a height-dependent function instead of a constant speed,  
198 which represents the annual average over more than 100 stations.

199

200 As part of this experiment, a polynomial model was also tried, in an attempt to improve the accuracy of the average ascent  
201 speed. The resulting displacements showed, however, very little improvement (i.e. smaller differences to GNSS measured  
202 displacements), indicating that the assumed vertically constant ascent rate of 5 m/s is a sufficient approximation.

203

204 As a next step, it is necessary to calculate the height profile from temperature and pressure information. For this step, we use  
205 the formula for a dry atmosphere with piecewise constant lapse rate (Alexander and de la Torre, 2011). Relative humidity  
206 could also be considered by using the virtual temperature, but it is often not available for early ascents and we also found  
207 that the differences in resulting displacements were small. For the first level, the International Civil Aviation Organization  
208 (ICAO) standard atmosphere lapse rate of -0.0065 K/m is used. For all subsequent steps, the temperature gradient is  
209 calculated directly from the temperature and pressure profile (mean values for each layer “i”).

210

211 The height profile is then used to calculate the time interval spent by the sonde between the noted levels. It can be estimated  
212 using the estimated vertical velocity mentioned earlier.

213 These time intervals are then used to determine the transport of the balloon according to the mean wind inside the layer  
214 between the levels  $i$  to  $i+1$ , see **Formula 4**.

215

216 Afterwards, this distance is converted into latitude and longitude using either the inverse Haversine method on an assumed  
217 sphere, or the forward transport function on the "WGS84" ellipsoid. The difference between the two transport functions is  
218 found to be practically invisible for smaller observed displacements (see **Figure 4**). Nevertheless, the ellipsoid option is used  
219 as it should deliver higher accuracy results. Finally, the resulting latitudes and longitudes are subtracted from the base  
220 coordinates to obtain the displacements.

221

222 Particular care is required when using reported wind direction near the North or South Pole. For example, when crossing the  
 223 North Pole, a radiosonde in a southerly airflow (prior to the crossing) finds itself in a northerly airflow (afterwards). So far,  
 224 only TAC has been used at the South Pole station, which means that the wind components are reported according to the  
 225 launch position, not to the actual position, and is thus constant during the ascent. We calculate the displacements in x and y  
 226 direction valid at this position and then convert that back to lat/lon positions and displacements.

227 The WMO Manual on Codes states that for stations within  $1^\circ$  of either pole wind direction shall be reported in such a way  
 228 that the azimuth ring shall be aligned with its zero coinciding with the Greenwich  $0^\circ$  meridian. There is currently an attempt  
 229 to update this advice for BUFR reports, such that wind direction should be reported relative to the current reported longitude  
 230 - to help in NWP use of such winds. Before comparing winds from the South Pole station with NWP fields they should have  
 231 their direction adjusted when the drift positions are calculated, but note this was not done in the present work.

232 Although the principle of displacement calculation is similar to the method presented in earlier work on this topic (Laroche  
 233 and Sarrazin, 2013), we use different input data for height information. Instead of using the average ascent time for each  
 234 standard level, we calculate the times for each available level using the mean lapse rate for the representative layer.

235 Aberson (2017) applied a similar approach for dropsondes, albeit with a different way of calculating the vertical velocity.

236 Both of these methods are successful and promising, and for the purpose of this method they have been used as the basis for  
 237 reconstructing the trajectories as best as possible.

### 239 3 Implementation and availability

240 The software necessary for the creation of calculated balloon trajectories can be found in the Python package rs-drift:

- 241 • <https://zenodo.org/records/10663306>
- 242 • <https://pypi.org/project/rs-drift/>

243 Examples on how to use it are available in all repositories as an IPython notebook “rs\_drift\_example.ipynb”.

244

245 In addition to the coordinates of the launch site or station in degrees latitude and longitude, the trajectory function requires  
 246 profiles of four input variables in the right units: temperature [K], pressure [Pa], zonal wind (u) [m/s], meridional wind (v)  
 247 [m/s]. It accepts only input which is sorted in ascending order.

```
248 trajectory = rs_drift.drift.trajectory(lat, lon, temperature, u, v, pressure)
```

249 The function returns the following output:

```
250 trajectory == [latitude_displacement, longitude_displacement, seconds_since_start]
```

251 All those output variables are numpy arrays, with one element for each pressure level - with the same length as the input  
 252 data. For PIBAL ascents, the geopotential height must be provided as an additional keyword parameter.

253



254 It is possible to experiment with input data. If humidity information is available, the virtual temperature can be used instead  
255 of the observed air temperature. Also if more information of the balloon's mean ascent rate is present, this should be used as  
256 input in the additional arguments. Any approach including proper quality control of input data that is available should be  
257 used to create the best possible estimation of the balloon drift.

258

259 The drift of the balloon and sonde compounds is introduced as "displacement" from the starting point (launch site). For  
260 simplicity, the displacements can be added to the base coordinates to obtain the vertical profile of positions of the balloon.

261

#### 262 **4. Validation with GNSS radiosondes**

263 Validation per se is only possible when a trusted source can provide a good reference. Such is the case for modern sondes  
264 equipped with GNSS receivers, when it comes to the recovery of the balloon trajectories. For pre-GNSS radiosondes, a  
265 similar validation would be possible, if only one had available the information about the balloon trajectory. Unfortunately,  
266 this information is available only in rare cases.

267

268 The data from the modern GNSS radiosonde data encoded in the recent high-resolution BUFR files are used to verify the  
269 systematic and random errors of the calculated displacements at different pressure levels. This data set contains second-by-  
270 second records of actual positions of the sonde measured by GNSS in the form of displacements, thus enabling the direct  
271 comparison with the calculated displacements.

272

273 **Figure 4** also shows that the displacements obtained from GNSS and the displacements calculated from the wind data agree  
274 quite well. The small deviations likely come from differences between the actual (unknown) and assumed (5 m/s) ascent  
275 rate.

276

277 **Figure 5** provides an overview how large the displacements typically are and gives profiles of uncertainty estimates for the  
278 calculated displacements. In the troposphere the RMSE is mostly below 0.02 degrees (2.5 km), in the stratosphere it can be  
279 up to 0.1 degrees (12 km). These numbers amount to uncertainties of about one part in five to ten, of the observed variations  
280 (RMS), in the example shown. Still, this is much better than just ignoring the displacement.

281

282 These results were obtained by using as input the high-resolution data. For historical radiosondes, only comparatively low-  
283 resolution information is available (in the form of mandatory plus significant levels).

284 In **Figure 6** and **Figure 7**, the impact of using only mandatory and significant level information is shown. The difference of  
285 displacements in **Figure 6** is minimal, although the displacement is relatively large.

286 **Figure 7** shows a case of larger differences in relative terms. The overall zonal displacements are large and the winds vary  
287 strongly with altitude. An issue arises when selecting data points with low representativeness from the ascent, particularly  
288 those that are far from the layer average. This can result in less accurate outcomes compared to using averages from less  
289 detailed data. Figure 7 provides a good example of this issue with the  $v$  component of wind at original resolution and  
290 mandatory pressure levels only. The method of calculating the displacements itself uses mean wind speeds within the  
291 considered levels. Thus, if the observations are also means of larger vertical height differences, more or less randomly  
292 observed peaks become a smaller source of error.

293 Figures 6 and 7 respectively show the range of accuracy of the calculated trajectories quite well. The final displacements  
294 may differ in quality depending on the quality of the observations, the representativeness of the available levels, and the  
295 vertical resolution. All ascents in the validation examples had displacements, which added value in bringing the observation  
296 closer to the true position. The accuracy may vary based on the aforementioned input variables. However, we did not find  
297 any case where using the displacements would lead to a worse position estimate.

298

299 **Figure 8** shows the comparison between the displacements of two different data sets - on high resolution BUFR levels and  
300 on the other hand on mandatory levels only. It can be seen that for this subset of ascents there is still much value in the  
301 displacements for the mandatory levels only version. However, it should be noted that more available levels always lead to  
302 better results and the highest possible number should be used in any case.

303

304 Many of the older observational reports contain temperature and wind data on different levels. Only at mandatory levels both  
305 variables are available. In this case, interpolation can be performed for the points in between. When applied to IGRA data,  
306 wind data are interpolated to levels of the temperature observations. This allows the input to be maximised to calculate the  
307 best possible displacements.

308

## 309 **5. Evaluation with ERA5**

310 To evaluate the impact of taking the displacements into account, we compared the observed values from the radiosondes  
311 with the gridded ERA5 data, in one case assuming a strictly vertical ascent, and in the other case assuming an ascent along  
312 the calculated (slanted) trajectory defined by the displacements. The ERA5 fields at hourly resolution and  $1^\circ \times 1^\circ$  horizontal  
313 resolution were interpolated linearly horizontally to the observations locations defined in either of the two cases mentioned  
314 earlier (vertical or slanted).

315 These tests and comparisons used the short term forecast of the ERA5 assimilating model, also referred to as "background".  
316 This choice, instead of using ERA5 analyses, was made to try to maintain as much independence as possible with respect to  
317 the observations. This choice should largely avoid possible problems resulting from the fact that the observations are also  
318 assimilated into the ERA5 data, given that many other observations were assimilated alongside radiosondes and also

29

30

319 influenced the analysis state. Experimental comparisons to the ERA5 analyses (in contrast to background forecasts) showed  
320 that the analysis data fits significantly better with the vertical trajectory of observation than with the slanted version. This is  
321 to be expected, since radiosondes were assimilated as vertical profiles in ERA5.

322

323 **Figure 9** shows the benefit of comparing the radiosonde observations with the *background forecasts* as slanted profiles  
324 instead of vertical profiles. In low layers (below 700 hPa), the displacements are relatively smaller than at higher levels, and  
325 therefore hardly lead to deviations for temperature. In most cases, there is an improvement at levels located above 750 hPa,  
326 though at some stations the improvement is visible already as soon as the sonde reaches 850 hPa, depending on the wind  
327 speed and topography around the station. Typically, the effect is largest in regions with high upper-level wind speeds.  
328 Taking the displacements into account improves the background departure statistics between measurements and ERA5 not  
329 only for temperature but also wind and relative humidity.

330

331 For relative humidity, the improvement is confined to levels located below 250 hPa. Above this level, the relative humidity  
332 is generally very low, making it difficult to detect any meaningful difference with respect to the ERA5 background.

333 It is also important to note that some stations, where the RMSE of the ascents do not show signals of improvement in  
334 temperature, often still show improvement in humidity or wind (or vice versa).

335

336 Considering that radiosonde observations make up a larger part of the total observations for the reanalysis in earlier years,  
337 one might think that especially for these years the displacements are more relevant. The data investigation reveals that  
338 improvements of the departure statistics are not greater for earlier ascents than for more recent ascents. The reason might be  
339 that reanalysis fields before the satellite era are more strongly dependent on radiosondes. At these times few other upper-air  
340 observations were available, and radiosonde data were assimilated assuming vertically straight ascents. However, the density  
341 of the input data and the general quality of the reanalysis increased over the time, while the bias in measurements of the  
342 uppermost levels decreased over time. Therefore, the relative importance of representation uncertainties, with respect to the  
343 two other sources of uncertainties in the comparison (radiosonde instrumental uncertainties and ERA5 background  
344 uncertainties), is larger for more recent ascents. **Figure 10** shows that considering the displacements is beneficial, although  
345 to a lesser extent, also in the early days, when little upper-air information other than radiosondes was available.

346

347 Finally, in **Figure 11** there are the results of a global comparison for the year 2000 - like the previous ones, but calculated for  
348 all the available stations. A positive difference again indicates improvement due to taking the displacements into account.

349

350 To give a better insight, the differences of the RMSE are also plotted on a map for the 150 hPa level in **Figure 12**. Warm  
351 colours show improvement for the respective station by applying the displacements, cold colours show a deterioration.

352 Improvement clearly predominates for the majority of stations. Deteriorations in quality appear less frequent and of smaller  
353 magnitudes than improvements.

354

355 **Figure 13** shows the difference of the ERA5 background eastward wind speed in the 1990s at the station location minus the  
356 same wind speed at the displaced location. The differences are sizable in some regions. For example, the weaker wind speeds  
357 above station locations in China would indicate systematically too high observed wind speeds. This effect is large enough to  
358 explain some of the radiosonde wind minus background wind differences, as pointed out by Tenenbaum et al. (2022). This  
359 stresses again the importance of avoiding position errors in historical radiosonde ascents. Without the adjustments, artificial  
360 trends in wind speed from radiosondes would be introduced in some regions when switching from traditional to GNSS  
361 radiosondes.

362

## 363 **6. Evaluation with data assimilation experiments**

364 Desroziers et al. (2005) proposed a method to diagnose uncertainty statistics of observations in a data assimilation  
365 framework. As indicated in their work, there are important assumptions associated with the approach. Bias contributions  
366 aside, the overall level of uncertainties may be incorrect if, for example, there is significant correlation between observation  
367 random uncertainties and random uncertainties of the background that is used in the data assimilation. A separation of scales  
368 is indeed required in order to disentangle these two uncertainty components. Given the unique importance of radiosondes to  
369 inform on the state of the stratosphere in a background obtained from data assimilation, such as in a reanalysis (e.g.,  
370 Hersbach et al., 2020), there may be some components of the uncertainties (such as radiation) that are present, and possibly  
371 correlated, in the background and the observations. For these reasons, we do not use Desroziers' diagnostics in order to  
372 assign undisputable uncertainties to the radiosonde uncertainties. Instead, we use these diagnostics in order to detect any  
373 changes in the observation uncertainties, which include instrument and representativity uncertainties, owing to the effect of  
374 balloon drift.

375

376 To this end, we run two data assimilation experiments, using a simplified data assimilation setup. Simplifications are  
377 required in order to make such an undertaking numerically affordable. Otherwise, so-called 'full' data assimilation  
378 experiments, using all observations at the maximum resolution, are indeed too costly to conduct, if only for such an  
379 evaluation. The simplified data assimilation setup is based on the ECMWF Integrated Forecasting System (IFS) cycle 48R1  
380 configuration (ECMWF, 2023), using an octahedral reduced Gaussian grid with 159 wavenumbers, or approximately a  
381 horizontal resolution of 69 km, instead of the ECMWF operational configuration which has a resolution of approximately 9  
382 km at present. Also, similarly for affordability reasons, the experiments only assimilate conventional observations (no  
383 satellite observations), the number of four-dimensional variational (4D-Var) minimizations is reduced from three to two, and

384 the analysis increments are at a resolution of approximately 210 km (instead of 39 km for ECMWF operations). The  
385 simplified data assimilation setup enables us to run data assimilation experiments for a duration of two months, 01 June - 31  
386 July 1980.

387

388 The first experiment is the control. It assimilates the radiosonde observations as vertical profiles. The second experiment  
389 assimilates the radiosonde observations following the balloon trajectory when this information is available (otherwise the  
390 data are assimilated as vertical profiles). The balloon drift in the assimilation is handled by dividing the whole ascent into  
391 15-minute sub-profiles (Ingleby et al., 2018). In each sub-profile, the latitudes, longitudes, and times are invariant. In spite of  
392 this arrangement, which only partially reflects the true slanted nature of the profiles, we retain the terminology of “slanted  
393 profile” when discussing the results, for clarity within this paper.

394

395 We consider here the radiosonde observations that were assimilated in both experiments, to ensure no difference in results  
396 may be caused by sampling differences. **Table 4** shows the statistics for these data. For the reasons mentioned earlier, the  
397 interpretation of the table focuses on differences between the two experiments, and not on the absolute level of observation  
398 uncertainties determined by Desroziers’ diagnostics. Within 0.1 K, we find no detectable difference between the two  
399 experiments for the levels located below the 100 hPa pressure level. For levels located higher, i.e. pressure lower than 100  
400 hPa, one finds that background departures and estimated observation uncertainties are reduced in the experiment that  
401 assimilated the data along slanted profiles. This result is obtained for radiosondes launched from land stations as well as  
402 radiosondes launched from ships.

403

404 The differences may appear as very small and could be discarded as non important, if it was not for the fact that reducing  
405 observation and representation uncertainties is generally an impossible task, once observations were collected and processed  
406 already once. The present findings demonstrate that it is possible to generate greater return, in terms of information content,  
407 through a reprocessing of the observations. The reprocessing enables here to assimilate observations along a slanted  
408 trajectory. Furthermore, these are global statistics - see **Figure 14**. The previous sections indicated that results may vary per  
409 launch site. Consequently, the improvements shown here, for global statistics, must hide some greater improvements at some  
410 particular sites - see **Figure 15**.

411

412 Given previous results indicating a larger effect of the balloon drift during winter seasons (e.g. McGrath et al., 2006), and  
413 given the much greater number of radiosonde stations in the Northern Hemisphere as compared to the Southern hemisphere  
414 (e.g., see Figure 12), the present choice of the data assimilation season (Northern hemisphere summer, as Choi et al., 2015)  
415 represents a conservative approach. An impact of larger magnitude may be expected at different time periods, in particular  
416 during Northern hemisphere winter.

417

## 418 7. Discussion and conclusions

419 The verification and evaluation results have shown quite clearly that if at all possible, balloon displacements should be taken  
420 into account for all relevant data assimilation applications to minimise representation errors. Ignoring the possibility to  
421 account for observation location errors on the 100 km scale would be anachronistic, when global or regional reanalysis data  
422 sets approach spatial resolutions finer than 20 km.

423

424 The method to reconstruct the balloon position presented in this work is limited by a few assumptions and depends on the  
425 vertical resolution of the available profiles, and the conformance of the weather balloons to modern ascent speeds. For the  
426 applications tested, an attempt was made to obtain the best results globally, and a clear positive impact was found,  
427 particularly when comparing to ERA5 in the early 2000s, although positive results were also found at other times (e.g.,  
428 1980s). This is also consistent with other findings in similar settings where trajectory data are used to reduce representation  
429 errors (e.g., Laroche and Sarrazin, 2013).

430

431 The data assimilation experimental setup employed here is a simplified one, as compared to what may be used in a present-  
432 day reanalysis configuration such as ERA5. Yet, we observe a positive impact of the balloon drift in terms of reducing the  
433 background departures and the observation uncertainty, using Desroziers' diagnostics, for temperatures in the stratosphere.  
434 We expect that the quality of the corrections made to use radiosondes at a displaced horizontal position, as compared to  
435 using them at a vertical position, would increase when the background resolution and/or the background quality is increased.  
436 In addition, assessing the impact of the balloon drift sensitivity to the assimilation of other observations alongside  
437 radiosondes would be worth analysing. However, owing to time and computational constraints, it was not possible to  
438 investigate further these effects with full data assimilation experiments at higher horizontal resolution and using all available  
439 information, but we note this would be a useful pursuit.

440

441 The results of the tests have shown that the method is successful in reconstructing displacements and improving the accuracy  
442 of the atmospheric data. Whilst the additional information provided by the method may not always be a visible improvement  
443 for individual comparisons, it is of significant value when the displacement changes the gridbox of the model being  
444 compared. This has been demonstrated by improved means in the plots and better agreement between observations and  
445 ERA5.

446

447 The value of improving radiosonde observations by reprocessing of the positions was evaluated by conducting reduced-  
448 resolution data assimilation experiments, covering a two-month period in summer 1980. In the future, it would be desirable  
449 that the impact of similar activities that seek to improve the observational record be more regularly evaluated in the  
450 generation of downstream climate products. Such an evaluation should consider a longer time period and include the impact

451 on low-frequency variability in the products. For products such as reanalyses, obtained via data assimilation, this should  
452 entail full-resolution Observing System Experiments (OSEs). For other types of climate products, including those powered  
453 by new opportunities such as Artificial Intelligence or Machine Learning (e.g., Singh et al., 2022), it is important that  
454 mechanisms be found to evaluate the impact of using the observations and how changes made in their handling affects the  
455 outcome.

456  
457 Further experimentation using observation data from the period 2000 - 2020 is crucial and is likely to produce more  
458 compelling outcomes. The effective use of this method for informing future climate reanalysis is one of the main objectives.  
459 As the world faces increasing challenges related to climate change, the importance of accurate atmospheric data and the  
460 potential of new methods to improve it cannot be overstated. The use of improved position metadata with radiosonde  
461 observations can account for previously unexplainable phenomena, demonstrating the potential of this method to shed new  
462 light on atmospheric data analysis. In addition, the method has the potential to improve the accuracy of reanalyses and  
463 climate predictions, which are crucial for many socio-economic sectors.

464  
465 To achieve the optimal representation of the data, precise details regarding time and location must be available for every  
466 observation. One significant issue concerns the TAC format's transmission and storage of data, which often only includes a  
467 nominal timestamp such as 00:00 UTC or 12:00 UTC. However, the actual launch of the respective balloon in most cases  
468 took place 30-60 minutes earlier. The precise time difference from the nominal time is frequently unknown, therefore  
469 displacement information cannot be utilised to its fullest extent. Since temperature can vary by more than 1 K/hour in the  
470 boundary layer just due to the diurnal cycle this issue should be addressed. There are well known examples where changes in  
471 the sampling of the diurnal cycle introduced spurious trends into climate data products (Mears and Wentz, 2005). Whenever  
472 possible, the precise launch time should be used. In cases where this information is not available for individual ascents, the  
473 time difference between the nominal and actual launch can often be determined from earlier or later ascents. Operators are  
474 normally advised to minimise the variation throughout the launch procedure and, therefore, launch balloon sondes at the  
475 same time every day.

476  
477 Additional work to better understand the causes of variation in balloon ascent speeds (e.g., Zhang et al., 2019) could help  
478 further improve the results. Also, given all the uncertainty sources, it could be possible to generate an ensemble of  
479 trajectories for each ascent. Pendulum motion is an effect that would need to be better understood, as it could be of  
480 importance for example in geographical locations where wind advection leads to small horizontal displacements.

481  
482 The same approach as presented in this paper can be used to reprocess rocketsondes, dropsondes, ozonesondes, or any other  
483 in-situ sonde advected by the wind, provided the necessary information is available. Taking into account the accurate balloon  
484 position would also be beneficial when comparing radiosonde observations with GNSS radio occultation (RO) observations

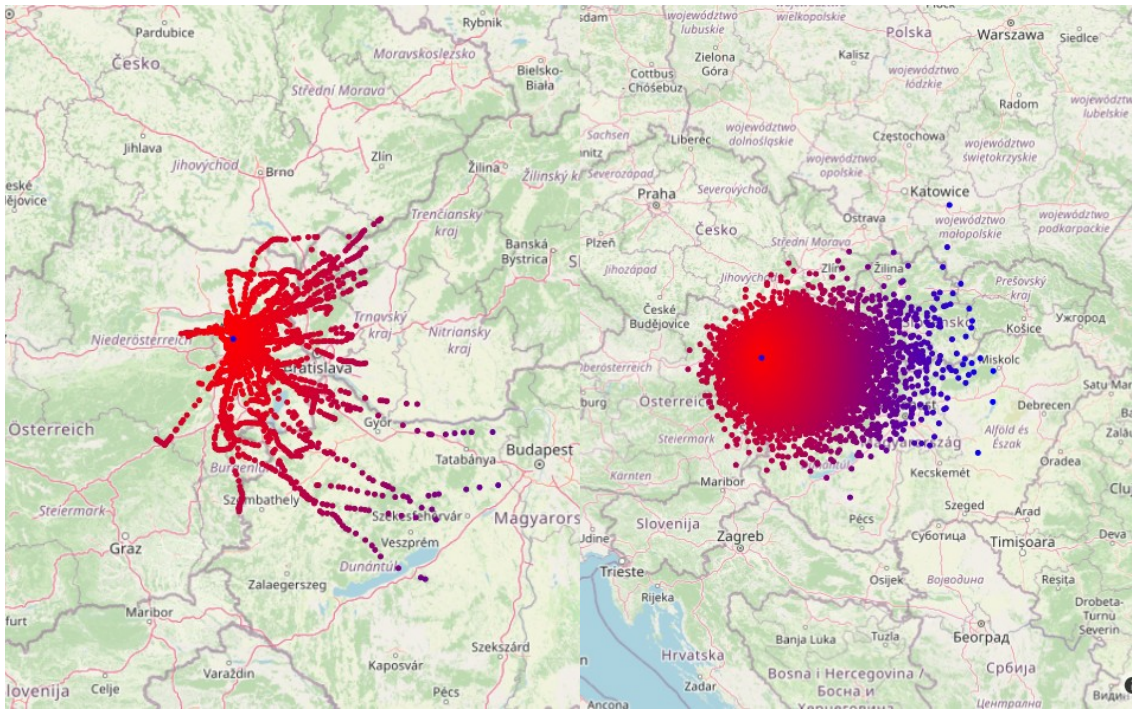
485 (Gilpin et al. 2018). Indeed, while it is established practice to consider the tangent point drift of the RO data (e.g., Poli and  
486 Joiner, 2004), radiosonde data is frequently presumed to move vertically only.

487

488 In conclusion, the development and testing of the method for reconstructing displacements based on the wind profile shows  
489 promising results. The results presented in this paper suggest taking balloon displacements into account when producing  
490 meteorological or climatological data based on upper-air in situ balloon-borne observations.



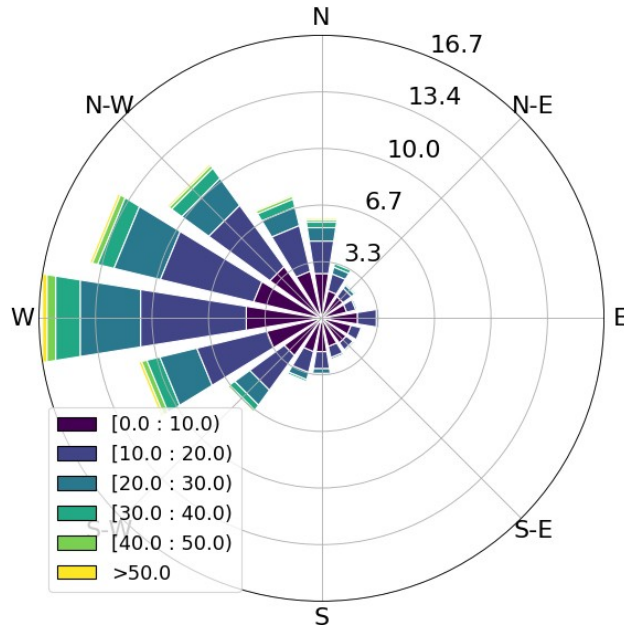
492 Appendices



493

494

© OpenStreetMap contributors 2023. Distributed under the Open Data Commons Open Database License (ODbL) v1.0.

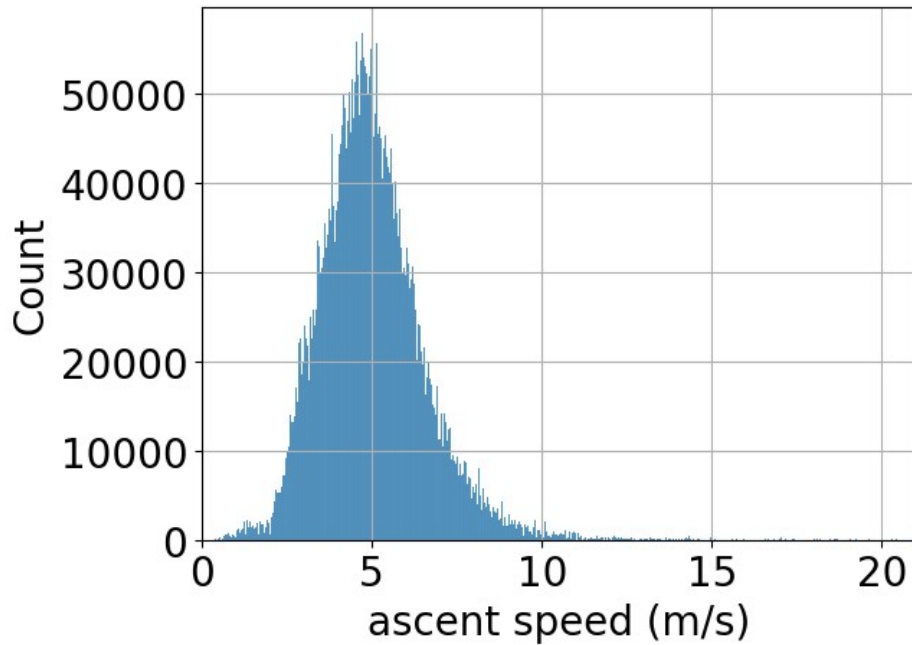


495

50

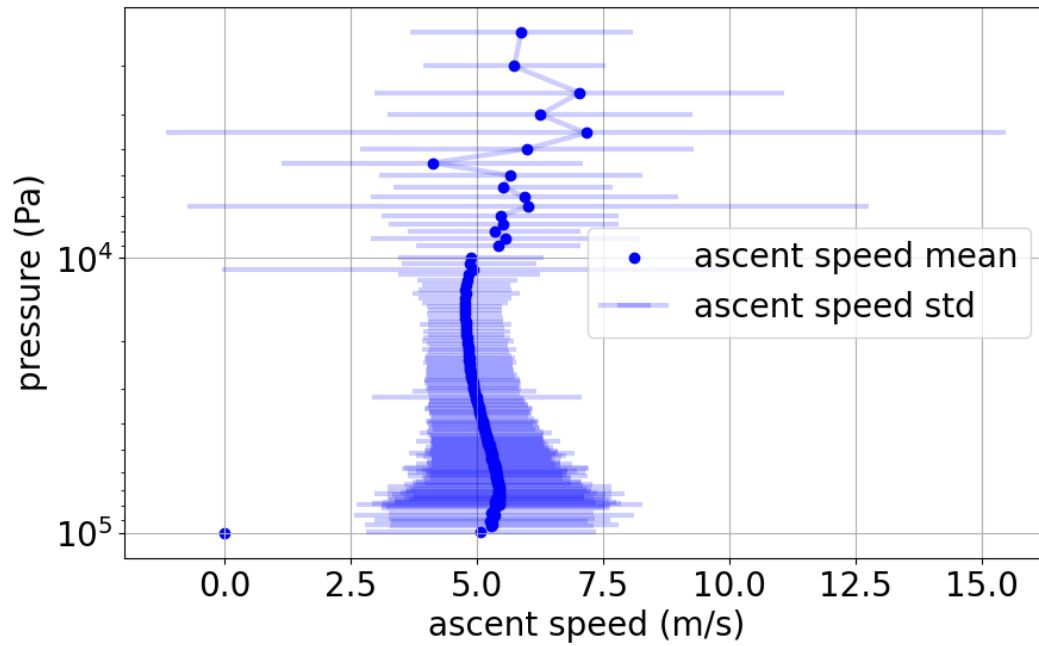
51

496 **Figure 1: Upper panels: Balloon displacements for station Vienna Hohe Warte, Austria (WIGOS ID 0-20001-0-11035). Central**  
 497 **blue dot denotes station location, other dots are balloon positions calculated from wind data as explained in text, coloured red to**  
 498 **blue with increasing distance. Note the area covered is non-isotropic around the launch site. Left panel: Trajectories of all**  
 499 **radiosonde ascents during the year 2000. Right panel – maximum displacements of all available ascents for all years between 1950**  
 500 **and 2021. Lower panel: windrose of Vienna Hohe Warte station for all available wind data. Colour indicates wind speed [m/s],**  
 501 **radius indicates frequency distribution [%] of direction, from where the wind comes from (sectors) and wind speed (colors).**



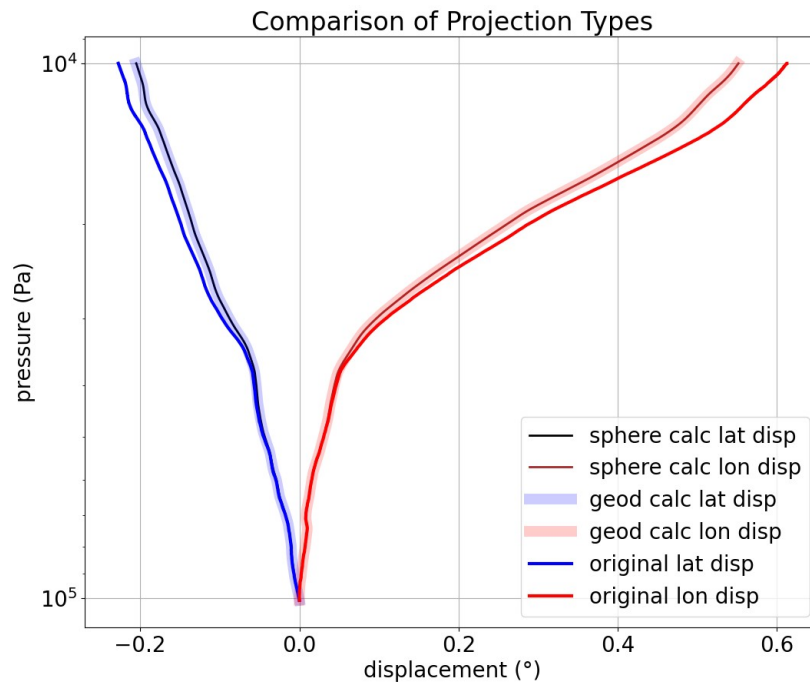
502

503 **Figure 2: The observed ascent speeds from a sample of approximately 10 million BUFR encoded observations with known altitude**  
 504 **time series in 2020.**



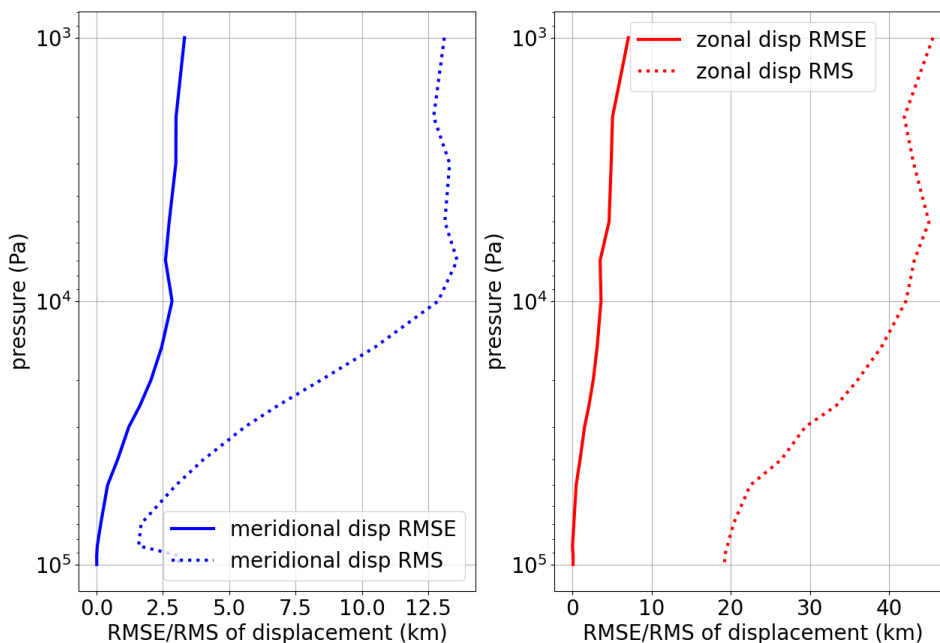
505  
506  
507

Figure 3: Mean ascent speed with standard deviation bars for all radiosonde ascents from Riverton USA, in 2020, derived from high resolution BUFR data.



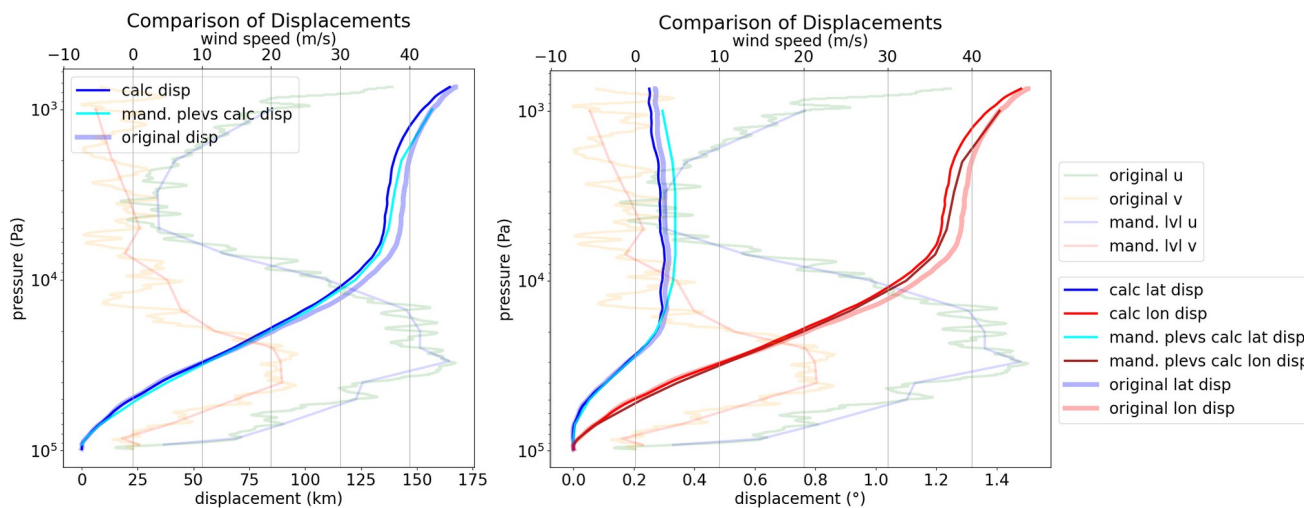
508  
509  
510  
511

Figure 4: Calculated displacements (black and brown for spherical earth, thick light blue and red for WGS84). Observed displacements stored in BUFR displacements (blue and red) are included for comparison. Tallahassee, Florida - USA 2020.05.31 23:19:00



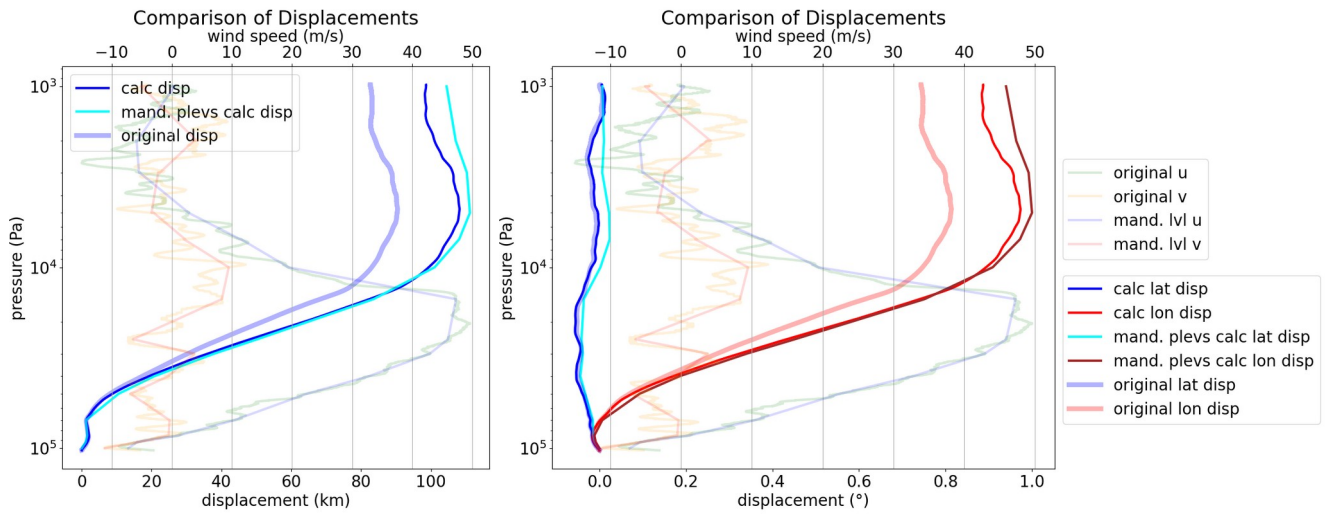
513  
514  
515  
516

**Figure 5: RMS of meridional (blue dotted) and zonal (red dotted) displacements and RMSE between observed (from GPS) and modelled displacements (solid blue and solid red, respectively). The samples contain all BUFR encoded ascents in the summer months of 2020 (more than 10000).**



517  
518  
519  
520  
521  
522

**Figure 6: Vertical profiles of displacements (starting at zero at surface), calculated from observed winds (thin lines) or taken from BUFR thick light lines. The profiles of observed wind (thin light colors) are plotted to the upper x axis - Peachtree City, Georgia - USA 31.01.2021 23:24:00. Left panel: overall displacements in km, right panel: lat and lon displacements in degrees as encoded in BUFR.**

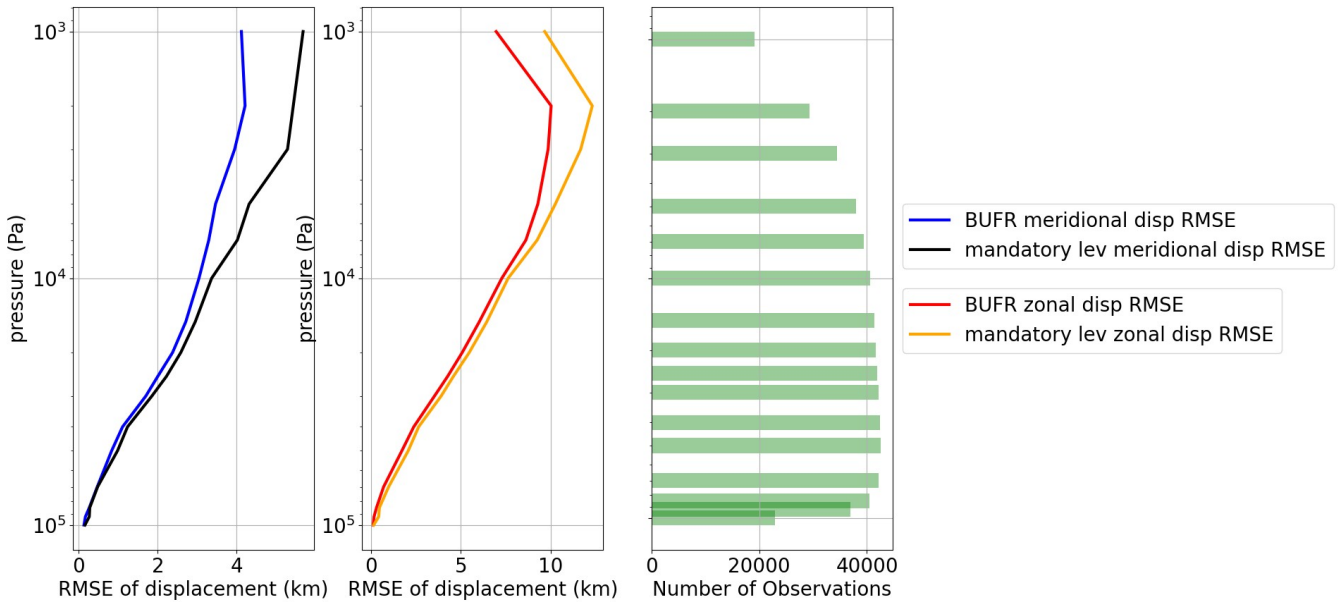


523  
 524 **Figure 7: Vertical profiles of displacements (starting at zero at surface), calculated from observed winds (thin lines) or taken from**  
 525 **BUFR thick light lines. The profiles of observed wind (thin light colors) are plotted to the upper x axis - Ishigaki, Okinawa - Japan**  
 526 **2019.12.31 23:31:00 . Left panel: overall displacements in km, right panel: lat and lon displacements in degrees as encoded in**  
 527 **BUFR.**

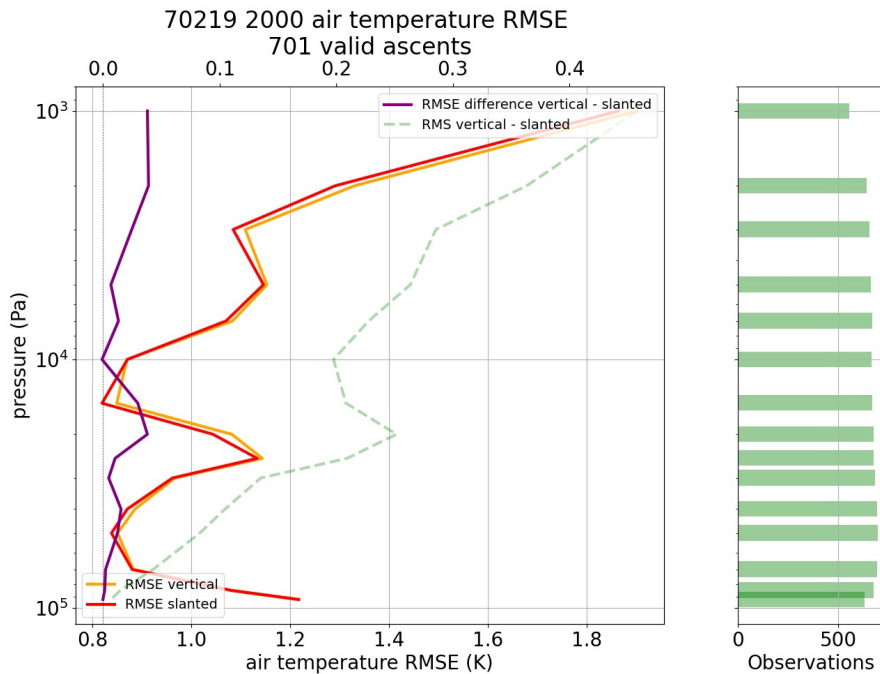
528

529

530

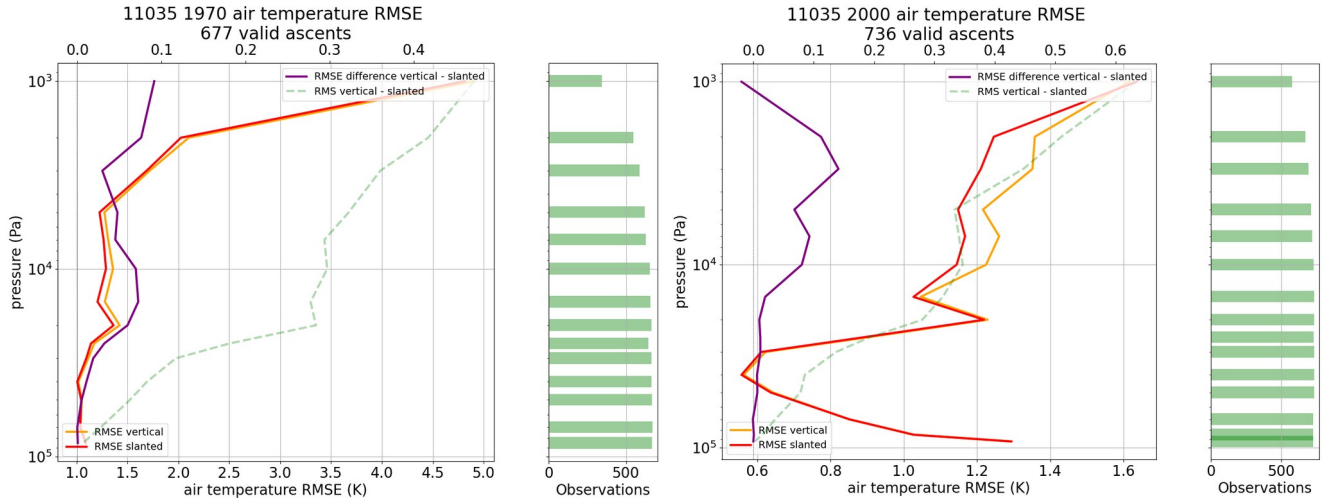


531 **Figure 8: RMSE between observed and modelled displacements of meridional (left panel) and zonal (right panel) components,**  
 532 **averaged over all stations available in October 2014, one of the first months with a sizable number of high-resolution BUFR**  
 533 **encoded profiles. Blue and red are RMSE profiles obtained by using the full vertical resolution of BUFR observations, black and**  
 534 **orange are RMSE profiles, and obtained by using only mandatory level information.**  
 535  
 536



537  
538  
539  
540  
541  
542

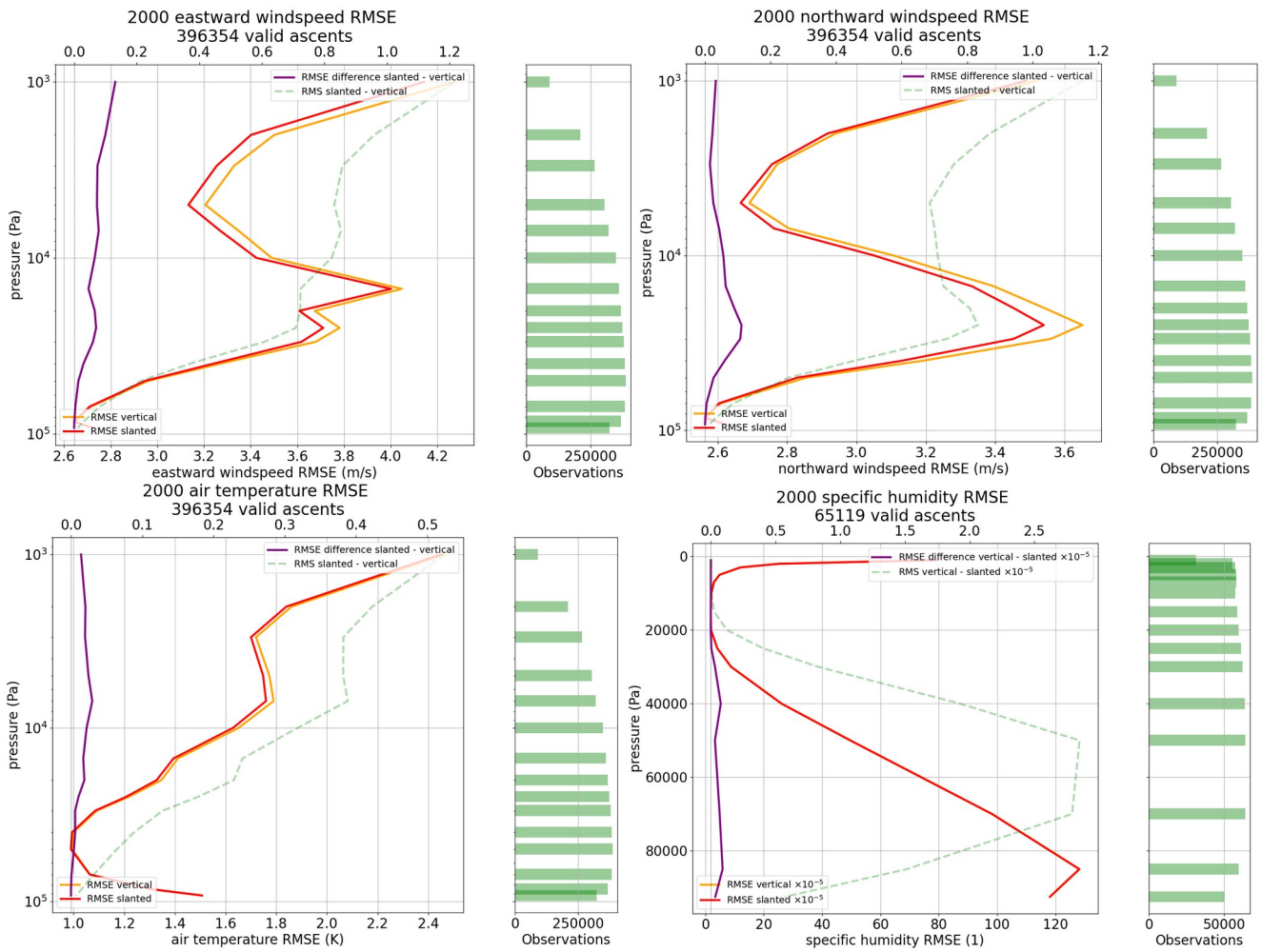
**Figure 9: Bethel Airport, Alaska all 2020 ascents. RMSE (obs - ERA5) of base coordinate temperatures minus sonde temperatures (orange) and RMSE (obs - ERA5) of displaced temperatures minus sonde temperatures (red), also RMS of displaced minus base (green dashed) to show the magnitude of difference between base and displaced temperatures. Positive difference between orange and red graphs (purple line, upper x axis) shows improvement due to more accurate balloon position. Green bars on the right indicate sample sizes at different levels.**



543  
544  
545  
546  
547

**Figure 10: Vienna Hohe Warte, Austria - Left: 1970 all ascents, Right: 2020 all ascents. Different x-axes scales are used. RMSE (obs - ERA5) of temperature assuming vertical ascents (orange, lower x-axis) and RMSE (obs - ERA5) of temperature from slanted ascents, taking balloon drift into account (red, lower x-axis). Positive difference between orange and red graphs (purple line, upper x axis) shows improvement due to more accurate balloon position.**

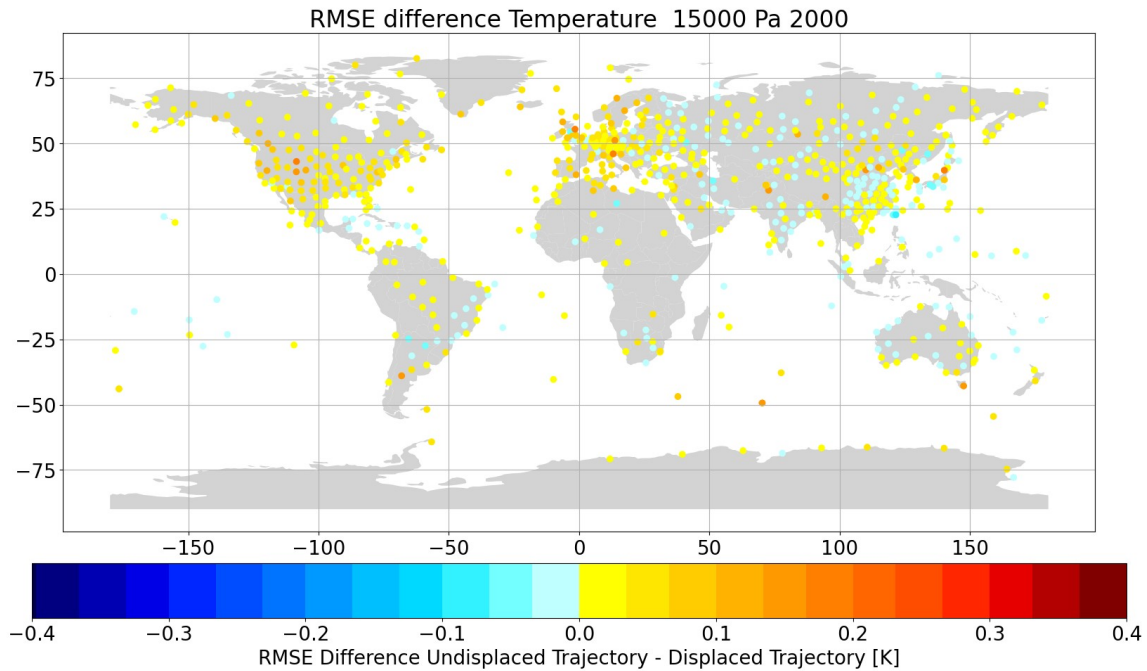
548



549

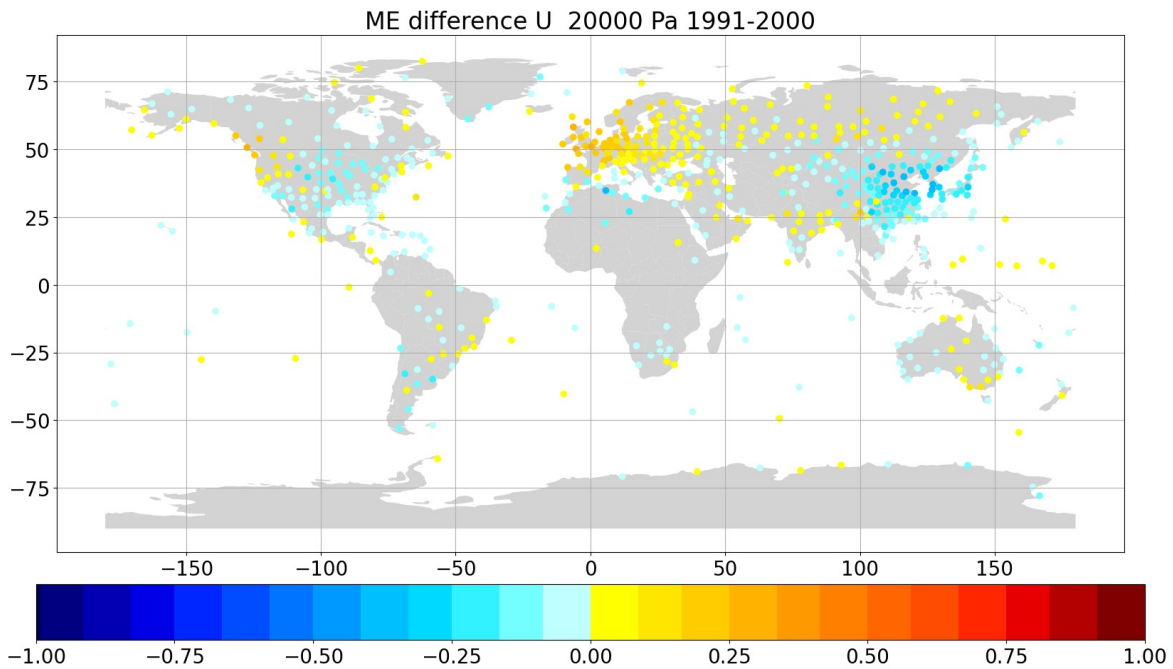
550

551 **Figure 11: Global RMSE (obs - ERA5 background) assuming vertical ascents (orange) and RMSE (obs - ERA5 background) from**  
 552 **reconstructed slanted ascents (red), calculated from all available ascents of year 2000. The differences between orange and red**  
 553 **graphs (purple line, upper x axis) shows how much the better balloon position improved the temperature data (positive =**  
 554 **improvement). The “RMS vertical - slanted” (green dashed line, upper x axis) indicates how much the ERA5 background varies**  
 555 **on average between the vertical and slanted balloon profiles. - Top left: u wind component; Top right: v wind component; Bottom**  
 556 **left: temperature; Bottom right: specific humidity in kg/kg (note scaling factor  $10^{-5}$ ).**



558  
559  
560  
561  
562

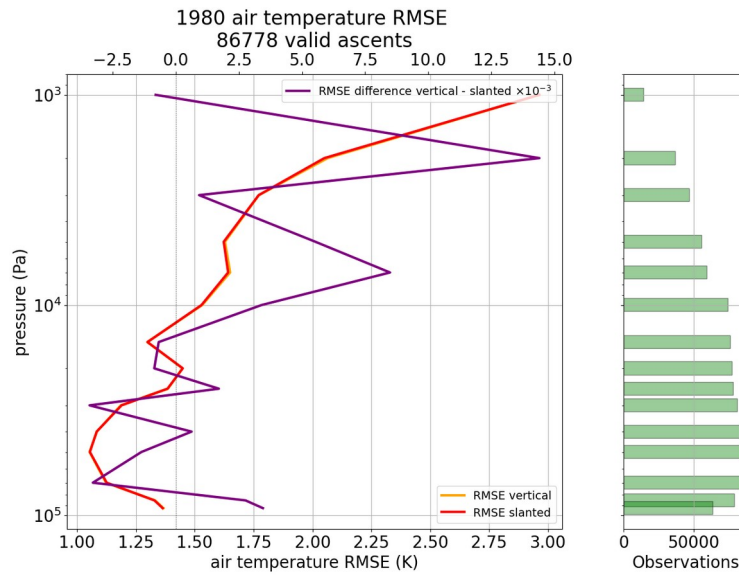
**Figure 12: Global stations difference of temperature [K] observation RMSE (obs - ERA5) when compared to background at station coordinates minus the temperature observation RMSE (obs - ERA5) when compared to background at displaced position - Positive values indicate improvement due to more accurate balloon position. All available observations at 150 hPa averaged over all ascents in the year 2000.**



563  
564  
565

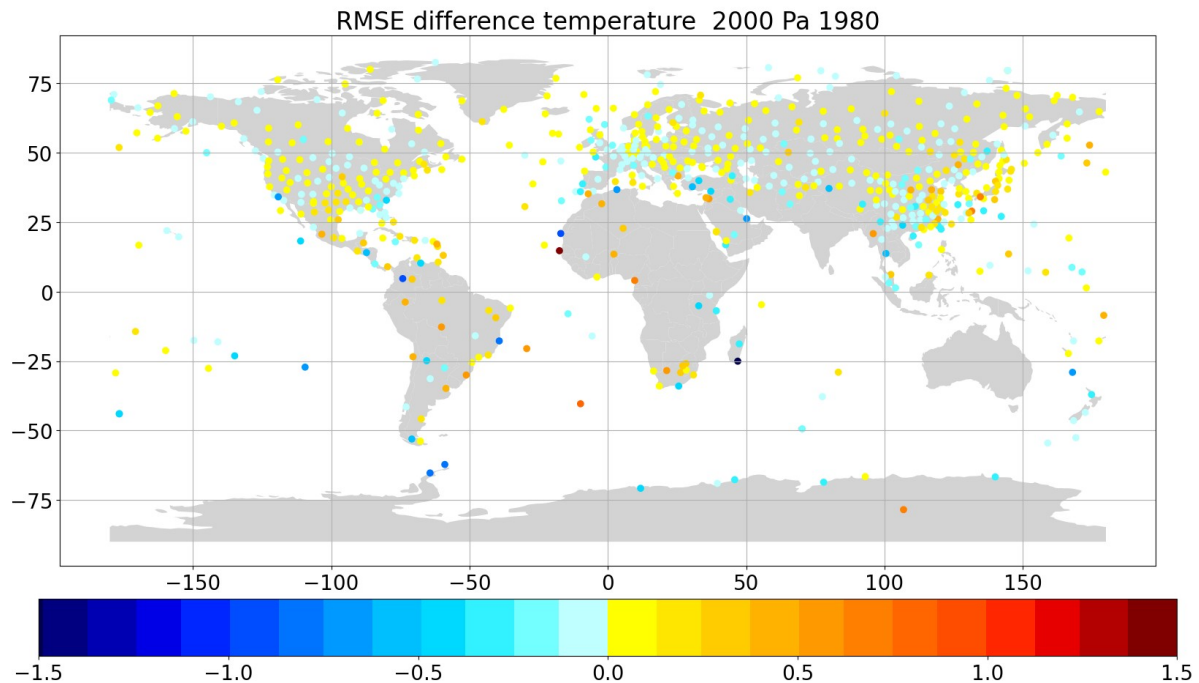
**Figure 13: Mean zonal (u) wind [m/s] difference obs - ERA5 background at station position minus obs - ERA5 background at displaced position. All available values on 200 hPa of years 1991 - 2000.**





566

567 **Figure 14: Air temperature obs-bg RMSE difference for experiment “vertical” (orange) and for experiment “slanted” (red). The**  
 568 **difference of differences (orange-red) yields the purple line, upper x axis, note scaling factor  $10^{-3}$ . Positive values indicate**  
 569 **improvement due to more accurate balloon position. All available stations on mandatory pressure levels between 1980.06.01-**  
 570 **1980.07.31.**



571

572 **Figure 15: Air temperature obs-bg RMSE [K] difference of experiment “vertical” minus RMSE of experiment “slanted”. Positive**  
 573 **values indicate improvement due to usage of more accurate balloon position. All available stations on 20 hPa between 1980.06.01-**  
 574 **1980.07.31.**

74

75

575 **Table 1: Ascent speed percentiles for a sample of 10.000.000 observations with known altitude time series in 2020.**

Percentile	Value	Unit
1	2.05	[m/s]
5	2.82	[m/s]
25	4.01	[m/s]
75	5.85	[m/s]
95	7.74	[m/s]
99	10.09	[m/s]

576

578 **Formula 1, 2: Calculation of the vertical gradient of temperature. See Table 2.**

$$579 \quad \Gamma_{(p)} = \frac{\delta T}{\delta z} = \frac{\delta T}{\delta p} \frac{\delta p}{\delta z} = \frac{-\delta T}{\delta p^\kappa} \frac{\delta p^\kappa}{\delta p} \frac{\delta p}{\delta z} \quad (1)$$

$$580 \quad \Gamma_{(p)} = \frac{-\delta T}{\delta p^\kappa} \frac{p^\kappa}{T} \frac{\kappa g}{R_d} \quad (2)$$

581

582

583 **Formula 3: Calculation of layer height. See Table 2.**

$$584 \quad \Delta z_{(i \rightarrow i+1)} = \frac{T_i}{\Gamma_i} \left( \frac{p_{i+1}}{p_i} \right)^{\frac{-\Gamma_i R_d}{g} - 1} \quad (3)$$

585

586

587

588 **Table 2: Height profile calculation. Explanation of all used variables.**

Symbol	Description	Unit	Data source
$\Gamma$	temperature lapse rate	[K/m]	observed variable
$p$	pressure	[Pa]	observed variable
$T$	temperature	[K]	observed variable
$\Delta z$	layer height	[m]	calculated variable
$\kappa$	isentropic expansion factor	[1]	$\kappa = R/c_p$
$C_p$	specific heat capacity of air at constant pressure	[J/kg/K]	constant (1005.7)
$R_d$	gas constant for dry air	[J/kg/K]	constant (286.7)
$g$	standard gravity	[m/s <sup>2</sup> ]	constant (9.80665)

589

590

591 **Formula 4: Transport of the balloon with the wind. See Table 3.**

$$\vec{s}_{(i+1)} = \frac{\vec{u}_{(i \rightarrow i+1)} * \Delta z_{(i \rightarrow i+1)}}{W_{balloon}} \quad (4)$$

592

593

594

595

**Table 3: Time interval calculation. Explanation of all used variables.**

Symbol	Description	Unit	Data source
$\vec{s}$	distance travelled	[m]	0 at $i = 0$ , lon for u, lat for v
$\vec{u}$	wind	[m/s]	observed variable, u and v components of wind
$\Delta z$	layer height	[m]	calculated variable
$w$	rate of ascension	[m/s]	5, prescribed variable

596

597

598 **Table 4: Statistics for the radiosonde observations actively used by both data assimilation experiments (vertical and slanted),**  
 599 **separating between radiosondes launched from land stations and radiosondes launched from ships. P indicates the pressure (hPa),**  
 600 **RSD indicates the robust standard deviation of background departures (i.e., before assimilation), SIGO indicates the estimated**  
 601 **observation uncertainty (see text for details), and N indicates the data count. Results that differ between the two experiments are**  
 602 **shown in bold and underlined. Observations that were used by only either one of the two experiments are excluded from these**  
 603 **statistics.**

Pressure level range	P ≥ 500 hPa		500 hPa > P ≥ 100 hPa		100 hPa > P ≥ 1 hPa	
Experiment	Vertical	Slanted	Vertical	Slanted	Vertical	Slanted
<b>Radiosondes from land stations</b>						
<b>RSD</b>	1.2 K	1.2 K	1.3 K	1.3 K	<b><u>2.1 K</u></b>	<b><u>2.0 K</u></b>
<b>SIGO</b>	1.1 K	1.1 K	1.2 K	1.2 K	<b><u>2.1 K</u></b>	<b><u>2.0 K</u></b>
<b>N</b>	31,027,909	31,027,909	30,229,363	30,229,363	1,358,298	1,358,298
<b>Radiosondes from ships</b>						
<b>RSD</b>	1.2 K	1.2 K	1.2 K	1.2 K	<b><u>1.6 K</u></b>	<b><u>1.5 K</u></b>
<b>SIGO</b>	1.1 K	1.1 K	1.2 K	1.2 K	<b><u>1.8 K</u></b>	<b><u>1.6 K</u></b>
<b>N</b>	838,265	838,265	669,655	669,655	34,709	34,709

605

606

**607 Code and data availability**

608 Radiosonde data used in the present work are available from <https://doi.org/10.7289/V5X63K0Q> (IGRA) and  
609 <https://doi.org/10.24381/cds.f101d0bf> (C3S CDS) and the National Centers for Environmental Information (NOAA NCEI)  
610 Radiosonde Archive (<https://www.ncei.noaa.gov/data/ecmwf-global-upper-air-bufr/archive/>). Climate reanalysis data  
611 (ERA5) are available from <https://doi.org/10.24381/cds.bd0915c6>. The code discussed in this paper is available from  
612 <https://doi.org/10.5281/zenodo.10663306>.

**613 Author contribution**

614 Ulrich Voggenberger and Leopold Haimberger designed the method to estimate balloon positions. Ulrich Voggenberger  
615 developed the code and optimised the estimations and calculations with further input from Federico Ambrogi. Ulrich  
616 Leopold Haimberger and Ulrich Voggenberger validated and evaluated the results based on ERA5 data. Paul Poli ran the  
617 data assimilation experiments and evaluated the results in section 6. Ulrich Voggenberger prepared the manuscript with  
618 contributions from all co-authors.

**619 Competing interests**

620 The contact author has declared that none of the authors has any competing interests.

**621 References**

- 622 Aberson, S. D., Sellwood, K. J., & Leighton, P. A.: Calculating Dropwindsonde Location and Time from TEMP-  
623 DROP Messages for Accurate Assimilation and Analysis. In *Journal of Atmospheric and Oceanic Technology* (Vol.  
624 34, Issue 8, pp. 1673–1678). American Meteorological Society. <https://doi.org/10.1175/jtech-d-17-0023.1>, 2017.
- 625 Alexander, P., and de La Torre, A.: Uncertainties in the measurement of the atmospheric velocity due to balloon-  
626 gondola pendulum-like motions. *Adv. Space Res.*, 47 (4):736-739, <https://doi.org/10.1016/j.asr.2010.09.020>, 2011.
- 627 Choi, Y., J. Ha, and G. Lim: Investigation of the Effects of Considering Balloon Drift Information on Radiosonde  
628 Data Assimilation Using the Four-Dimensional Variational Method. *Wea. Forecasting*, 30, 809–826,  
629 <https://doi.org/10.1175/WAF-D-14-00161.1>, 2015
- 630 Crutcher, H. L.: Distribution of radiosonde errors. NOAA Tech. Rep. Environmental Data and Information Service  
631 (EDIS), 32, [https://repository.library.noaa.gov/view/noaa/30830/noaa\\_30830\\_DS1.pdf](https://repository.library.noaa.gov/view/noaa/30830/noaa_30830_DS1.pdf), 1979.

- 632 Dabberdt, W. F., and Turtiainen, H.: Observations platforms: Radiosondes, in *Encyclopedia of Atmospheric Sciences*  
633 (Second Edition), eds. G. R. North, J. Pyle, F. Zhang, Academic Press, pp 273-284, ISBN 9780123822253.  
634 <https://www.sciencedirect.com/referencework/9780123822253/encyclopedia-of-atmospheric-sciences>, 2015.
- 635 Desroziers, G., Berre L., Chapnik B., and Poli, P.: Diagnosis of Observation, Background and Analysis-Error  
636 Statistics in Observation Space. *Quarterly Journal of the Royal Meteorological Society* 131, no. 613 (October 1,  
637 2005): 3385–96. <https://doi.org/10.1256/qj.05.108.>, 2005.
- 638 Durre, I., Yin, X., Vose, R. S., Applequist, S., Arnfield, J., Korzeniewski, B., and Hundermark, B.: Integrated Global  
639 Radiosonde Archive (IGRA), Version 2. NOAA National Centers for Environmental Information.  
640 <https://doi.org/10.7289/V5X63K0Q>, 2016.
- 641 Durre, I., Yin, X., Vose, R. S., Applequist, S., and Arnfield, J., 2018: Enhancing the Data Coverage in the Integrated  
642 Global Radiosonde Archive. *J. Atmos. Oceanic Technol.*, 35, 1753–1770, <https://doi.org/10.1175/JTECH-D-17-0223.1>.
- 644 Dutton, J. A.: *The ceaseless wind: An Introduction to the Theory of Atmospheric Motion*. Dover Publications, New-  
645 York, 617 pp., ISBN:978-0486495033, <https://doi.org/10.1029/88EO01137>, 1986.
- 646 ECMWF: IFS Documentation CY48R1. <https://www.ecmwf.int/en/publications/ifs-documentation>, last access 25-10-  
647 2023.
- 648 Favà, V., Curto, J. J., and Gilabert, A.: Thermodynamic model for a pilot balloon, *Atmos. Meas. Tech.* [preprint],  
649 <https://doi.org/10.5194/amt-2021-206.>, 2021.
- 650 Gilpin, S., Rieckh, T., and Anthes, R.: Reducing representativeness and sampling errors in radio occultation–  
651 radiosonde comparisons, *Atmos. Meas. Tech.*, 11, 2567–2582, <https://doi.org/10.5194/amt-11-2567-2018>, 2018.
- 652 Hersbach, H, Bell, B, Berrisford, P, et al.: The ERA5 global reanalysis. *Q J R Meteorol Soc.* 146: 1999–2049.  
653 <https://doi.org/10.1002/qj.3803>, 2020.
- 654 Hersbach, H., Bell, B., Berrisford, P., et al.: Characteristics of ERA5 and innovations for ERA6. Copernicus Climate  
655 Change Service General Assembly 2022. Available from  
656 [https://climate.copernicus.eu/sites/default/files/2022-09/S3\\_Hans\\_Hersbach\\_v1.pdf](https://climate.copernicus.eu/sites/default/files/2022-09/S3_Hans_Hersbach_v1.pdf), last access 26-03-2023.
- 657 ICAO Standard Atmosphere - ISA <https://www.foehnwall.at/meteo/isa.html>, last access 25-10-2023.
- 658 Ingleby, B., Pauley, A. Kats, J. Ator, D. Keyser, A. Doerenbecher, E. Fucile, J. Hasegawa, E. Toyoda, T. Kleinert,  
659 W. Qu, J. St James, W. Tennant, and R. Weedon,: Progress toward High-Resolution, Real-Time Radiosonde Reports.  
660 *Bull. Amer. Meteor. Soc.*, 97, 2149-2161, <https://doi.org/10.1175/BAMS-D-15-00169.1>. 2016.
- 661 Ingleby, B., Isaksen, L., Kral, T., Haiden, Th., and Dahoui, M.: Improved use of atmospheric in situ data. ECMWF  
662 Newsletter 155. <https://doi.org/10.21957/cf724bi05s>, 2018.
- 663 Ingleby, B., Motl, M., Marlton, G., Edwards, D., Sommer, M., von Rohden, C., Vömel, H., and Jauhiainen, H.: On  
664 the quality of RS41 radiosonde descent data, *Atmos. Meas. Tech.*, 15, 165–183, <https://doi.org/10.5194/amt-15-165-2022>, 2022.

666 Kats A., Balagourov A & Grinchenko V. (2005) The impact of new RF95 radiosonde, introduction on upper-air data  
667 quality in the North-west region of Russia. Poster Pw(07), TECO-2005, WMO/TD- No. 1265; IOM Report- No. 82.

668 Keyser, D., 2000: RAOB/PIBAL Balloon Drift Latitude, Longitude, & Time Calculation In PREPBUFR. Available  
669 from [https://www.emc.ncep.noaa.gov/mmb/data\\_processing/prepbufr.doc/balloon\\_drift\\_for\\_TPB.htm](https://www.emc.ncep.noaa.gov/mmb/data_processing/prepbufr.doc/balloon_drift_for_TPB.htm), last access 26-  
670 03-2023.

671 Kitchen, M.: Representativeness errors for radiosonde observations. Q. J. R. Meteorol. Soc., 115: 673-700.  
672 <https://doi.org/10.1002/qj.49711548713>, 1989.

673 Laroche, S., and Sarrazin, R.: Impact of Radiosonde Balloon Drift on Numerical Weather Prediction and Verification.  
674 Weather and Forecasting, 28 (3), 772–782. <https://doi.org/10.1175/waf-d-12-00114.1>, 2013.

675 McGrath, R., T. Semmler, C. Sweeney, and S. Wang,: Impact of balloon drift errors in radiosonde data on climate  
676 statistics. J. Climate, 19, 3430–3442, <https://doi.org/10.1175/JCLI3804.1>, 2006.

677 Mears, C. A., and Wentz, F. J.: The effect of diurnal correction on the satellite-derived lower tropospheric  
678 temperature. Science, 309, 1548–1551. <https://doi.org/10.1126/science.1114772>, 2005.

679 Murillo, J., Mejia, J., Galvez, J., Orozco, R., and Douglas, M.: Quality control of pilot balloon network data for  
680 climate monitoring. Amer. Meteorol. Soc. 15th Conf. Appl. Clim., 13th Symp. Meteorol. Obs. Instr., **JP1.30** ,  
681 <https://api.semanticscholar.org/CorpusID:56365106>, 2005.

682 OpenStreetMap: OpenStreetMap® is open data, licensed under the Open Data Commons Open Database License  
683 (ODbL) by the OpenStreetMap Foundation (OSMF). You are free to copy, distribute, transmit and adapt our data, as  
684 long as you credit OpenStreetMap and its contributors. If you alter or build upon our data, you may distribute the  
685 result only under the same licence. The full legal code explains your rights and responsibilities. Our documentation is  
686 licensed under the Creative Commons Attribution-ShareAlike 2.0 license (CC BY-SA 2.0). Available from  
687 <https://planet.openstreetmap.org>, 2023.

688 Poli, P., and Joiner, J.: Effects of horizontal gradients on GPS radio occultation observation operators. I: Ray tracing.  
689 Q.J.R. Meteorol. Soc., 130: 2787-2805. <https://doi.org/10.1256/qj.03.228>, 2004.

690 Seidel, D. J., Sun, B., Pettey, M., and Reale, A.: Global radiosonde balloon drift statistics, J. Geophys. Res., 116,  
691 D07102, <https://doi.org/10.1029/2010JD014891>, 2011.

692 Singh, M., Kumar, B., Chattopadhyay, R., Amarjyothi, K., Sutar, A.K., Roy, S., Rao, S.A., and Nanjundiah, R.S.:  
693 Artificial intelligence and machine learning in earth system sciences with special reference to climate science and  
694 meteorology in South Asia. Current Sci., **122** (9), <https://doi.org/10.18520/cs/v122/i9/1019-1030>, 2022.

695 Steinacker, R., et al.: Unstationary aspects of Föhn in a large valley. Meteorology and Atmospheric Physics volume  
696 92, pages 255–284 (2006). <https://doi.org/10.1007/s00703-005-0134-y>, 2005.

697 Stohl, A.: Computation, accuracy and applications of trajectories - A review and bibliography, Atmos. Env., **32** (6),  
698 [https://doi.org/10.1016/S1352-2310\(97\)00457-3](https://doi.org/10.1016/S1352-2310(97)00457-3). 1998

699 Tenenbaum, J., Williams, P.D., Turp, D., Buchanan, P., Coulson, R., Gill, P.G., et al.: Aircraft observations and  
700 reanalysis depictions of trends in the North Atlantic winter jet stream wind speeds and turbulence. Quarterly Journal  
701 of the Royal Meteorological Society, 148(747), 2927–2941. <https://doi.org/10.1002/qj.4342>, 2022.

702 Tschannett, S.: Objektive hochaufgelöste Querschnittsanalyse. Diplomarbeit, Univ. Wien,  
703 <https://www.univie.ac.at/img-wien/>, 2003.

704 WMO: Guide to Instruments and Methods of Observation Volume I: Measurement of Meteorological Variables ,  
705 Commission for Instruments and Methods of Observation (CI-MO) Guide, WMO Pub. 8. Available from  
706 <https://library.wmo.int/records/item/41650-guide-to-instruments-and-methods-of-observation>, 2021.

707 Zhang, J., Chen, H., Zhu, Y., Shi, H., Zheng, Y., Xia, X., Teng, Y., Wang, F., Han, X., Li, J., et al.: A Novel Method  
708 for Estimating the Vertical Velocity of Air with a Descending Radiosonde System. Remote Sens. **11**, 1538.  
709 <https://doi.org/10.3390/rs11131538>, 2019.